Scientia Iranica B (2018) 25(1), 253–265

Sharif University of Technology
Scientia Iranica
Transactions B: Mechanical Engineering
http://scientiairanica.sharif.edu

Experimental study of fuel regression rate in an HTPB/N_2O hybrid rocket motor

H. Rezaei[a], M.R. Soltani[b,*], and A.R. Mohammadi[a]

a. *Space Transportation Research Institute, Iranian Space Research Center, Tehran, Iran.*
b. *Department of Aerospace Engineering, Sharif University of Technology, Tehran, P.O. Box 11365-11155, Iran.*

Received 13 May 2016; received in revised form 16 September 2016; accepted 19 December 2016

KEYWORDS
Hybrid motor;
Regression rate;
Oxidizer;
Fuel;
Pressure.

Abstract. The performance of an HTPB/N_2O hybrid motor was experimentally investigated. A hybrid motor was designed and manufactured in a laboratory with the purpose of studying the effects of various parameters on the motor's performance, including fuel regression rate and specific impulse. A series of tests were conducted to find a correlation between the fuel regression rate and the oxidizer's mass flux. The effects of chamber's pressure on the regression rate as well as other performance parameters were investigated. While the burning rate did not change dramatically, both the efficiency and ISP of the motor increased. The local fuel regression rate and the fuel port were also calculated. In addition, instantaneous regression rate was calculated using a special technique.

1. Introduction

A hybrid rocket motor is a type of chemical propulsion system, a combination of a solid rocket motor and liquid engine. In the classical form of hybrid motor, the solid fuel is embedded in the combustion chamber while the oxidizer, stored in a separate tank in gas or in liquid phase, is injected into the combustion chamber during operation of the motor (Figure 1).

The injection of oxidizer into the combustion chamber, followed by its mixture with the vaporized fuel, produces diffusion flames over the surface of the fuel (Figure 2) [1]. Heat transference from the surface of the flame to the fuel causes continuity of fuel evaporation and sustainability of the combustion. The existence of free space prior to the grain causes complete evaporation of the oxidizer in the combustion chamber before it reaches the grain; hence, the oxidizer enters the port in its gas phase from the beginning. This will cause uniform burning along the grain port, increasing the combustion efficiency. Moreover, this type of chamber configuration improves flame stability, resulting in a decrease in combustion instability by creating a vortex in this region. This chamber, known as the pre-combustion chamber, is considered in most of the experimental and operational hybrid motors [2,3]. According to Figure 2, there is a limited free volume (known as the post-combustion chamber) between the end of the grain and throat of the nozzle, providing sufficient time for better mixing and burning processes. Therefore, the unburnt fuel and the grain will mix with the oxidizer prior to being burnt in this zone, leading to an increase in the efficiency and specific impulse of the motor.

Hybrid motor is more controllable, more eco-friendly, and more secure than solid rocket. It also gives the ability to turn it off and restart. Compared to liquid engines, hybrid motor is less complex, less expensive,

*. *Corresponding author. Tel.: +98 21 66022731; Fax: +98 21 66022731*
E-mail address: msoltani@sharif.edu (M.R. Soltani)

doi: 10.24200/sci.2017.4317

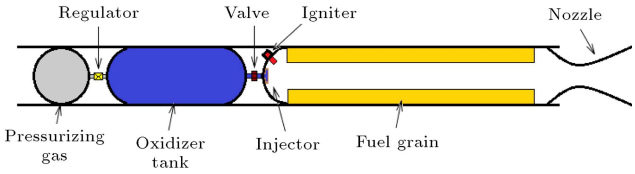

Figure 1. Schematic of a conventional hybrid motor.

and safer. Although hybrid motor is employed less than solid and liquid engines are, the research conducted over the past couple of years regarding its usage in various vehicles has been increasing rapidly. This has led to the operational use of hybrid motors in such cases as the Space ship1, which was operated in 2004 with the goal of carrying humans to the height of 100 km [4]. Recently, a second version of this vehicle was tested to carry seven space tourists. Ongoing research in this field includes analytical and numerical modeling to gain better understanding of the processes [5-7], small-scale experiments [8-10], and full-scale tests [11-12]. The main purposes of these research studies are to increase both the fuel regression rate and the efficiency of the motor's performance.

One of the main fuel options in the hybrid motor is HTPB along with an oxidizer such as gaseous or liquid O_2, H_2O_2, and N_2O. The N_2O, due to its self-pressurizing property, requires no pumping system during the flight, making the motor less complex and lighter. Furthermore, N_2O is inexpensive, extremely safe, non-toxic, and can be stored at ambient temperature. These features outweigh the slightly inferior performance of N_2O when compared to that of liquid oxygen or other hazardous alternatives.

A considerable number of researches have been done on the recognition of the performance of hybrid motor. However, in most cases, the gaseous oxygen is used due to its accessibility, handleability, and oxidizer's mass flow rate measurement [13-15]. To the best of the authors' knowledge, only a few number of scientific sources have been devoted to the use of N_2O in open literature, despite its wide usage in the propulsion applications.

Peretz et al. designed and constructed a lab-scale hybrid motor with HTPB fuel and N_2O oxidizer and investigated the effects of increasing the percentage of ammonium perchlorate within the fuel on the regression rate [16]. Their results indicated an increase in the regression rate with AP addition.

The regression rates of several types of fuels were studied by using N_2O as oxidizer. As a result, a correlation between regression rate and mass flux of the oxidizer through the port was obtained. Furthermore, the effect of addition of Al powder to the fuel on the regression rate was studied [2,17].

A numerical code was constructed to study the scale effect in an HTPB/N_2O hybrid motor [18]. This code solved Navier-Stokes equations by using a two-step, five-species combustion model; it further calculated the pressure of the chamber and the corresponding thrust. The simulated pressure and the thrust variations were both compared with the experimental results, and a fine accord was obtained. It is worth mentioning that the local regression rate and the fuel port were also calculated using this code.

In [19], scale rules in a hybrid motor were calculated by using a theoretical dimensional analysis. Additionally, series of experiments using PMMA/Gox were carried out on a laboratory-scale motor. Experimental and theoretical results for the key performance parameters such as the regression rate, O/F, and thrust, were in good agreement.

Seemingly, there are many unknowns regarding the use of N_2O for these types of motors. Therefore, the aim of this study was to gain further information about this specific motor, with a particular combination of fuel and oxidizer. In this paper, the fuel regression rate in an HTPB/N_2O hybrid motor is studied, and the effects of various factors on the regression rate and other parameters of the motor's performance, such as the specific impulse, are observed.

2. Experimental apparatus

An experimental set-up was designed, manufactured, and calibrated for this investigation. The stand had various components, including an experimental-scale

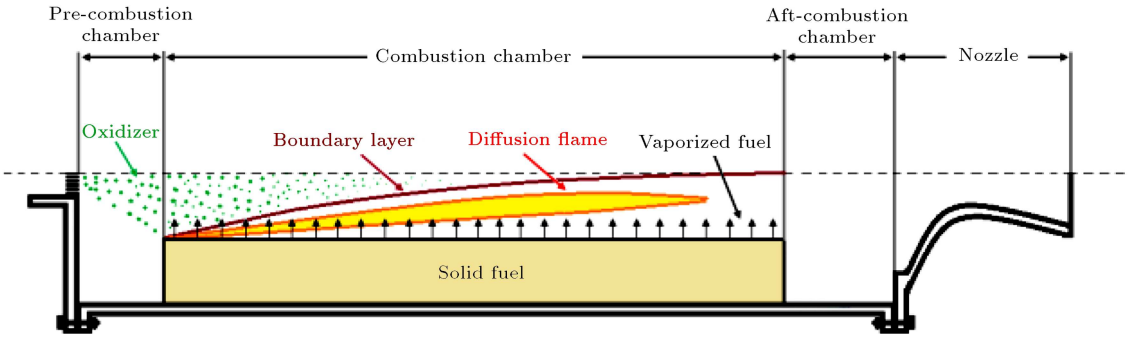

Figure 2. Evaporation and combustion process in a hybrid motor [1].

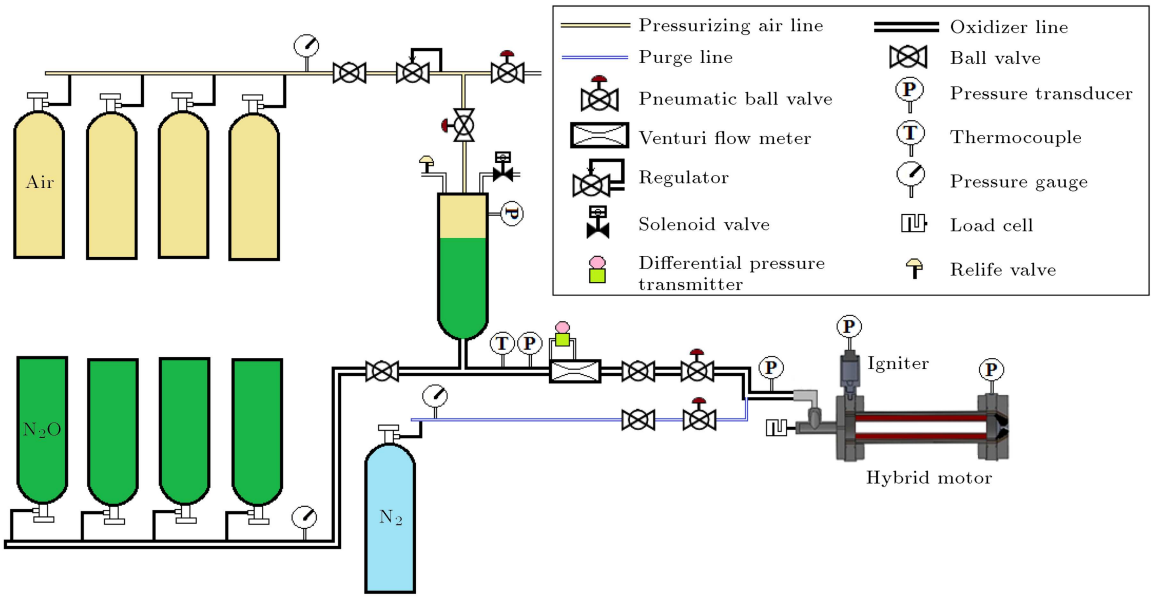

Figure 3. Layout of experimental set-up.

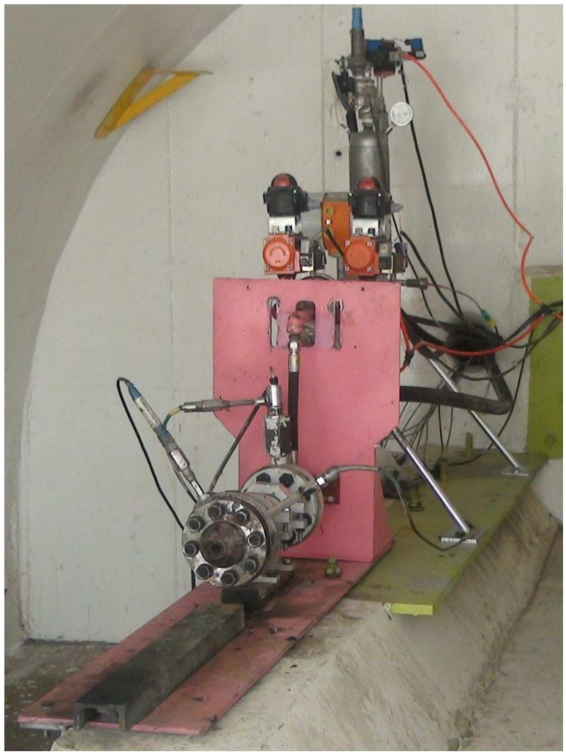

Figure 4. The experimental set-up of the present hybrid motor.

motor, an oxidizer tank, an oxidizer feeding system, purge line, thrust stand, data acquisition, reduction, and recording equipment. Figures 3 and 4 show a schematic and an image of the test stand.

2.1. The experimental motor

The experimental motor consisted of a central tube that was closed at both ends with two flanges (Figure 5). The igniter, the injector plane, and a converging-diverging nozzle (which was made of special material) were located on the primary and final flanges, respectively. Two empty spaces that respectively played the roles of an evaporation oxidizer chamber (pre-combustion chamber) and a mixing and combustion completion chamber (post-combustion chamber) were considered before and after the fuel grain. Motor tube was covered with an insulating layer, and the interior surfaces of the metal body within the pre-combustion and post-combustion chambers were coated with graphite pieces to protect them against the flames. The experimental motor was designed such that it could easily embed various amounts of fuel, and that different types of injectors could be installed on the motor.

2.2. The oxidizer feeding system

In this study, N_2O was used as an oxidizer. The gas (air) pressurizing method was utilized in order to pump the oxidizer. The feeding system included a high-pressure air tank, oxidizer storage tanks, oxidizer feeding line, pressurizing line, a run tank, a lateral purge line, manual and control valves, and various measuring sensors. The oxidizer in the tank was pressurized to about 10 bars higher than its vapor pressure to prevent flow cavitation in the line so that measuring the flow rate would be possible.

2.3. Igniter

A pyrogen igniter, which contained a small amount of composite solid fuel, was used to activate the fuel and to start the motor. The igniter was activated by embedding an electrical resistor within the fuel.

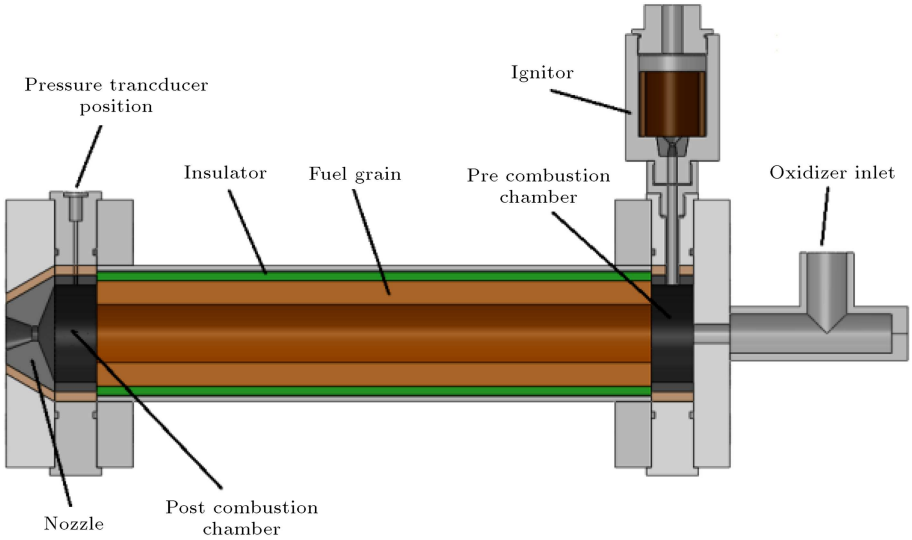

Figure 5. Layout of the present hybrid motor.

2.4. Measurements and data acquisition

Accurate pressure transducers with a full-scale precision of ± 0.5% and with an acquisition frequency of about 50 kHz were used to measure the pressures of the N_2O tank and the oxidizer before the injector and the combustion chamber. In addition, a load cell capable of measuring force was used to measure the thrust.

The oxidizer flow rate was measured by means of a sub-critical venturi. The mass flow rate was attained by measuring the pressure in the upper stream and at the venturi's throat. Prior to being used, the venturi was calibrated with a precision flow meter.

For data acquisition, an analog to digital (A/D) board, data acquisition software, and a computer were used. All data were acquired by means of an A/D board and were transferred to a PC computer for processing and analyzing.

The uncertainties in the specific impulse and efficiency of the motor depend on the measured thrust, pressure of the chamber, and oxidizer mass flow rate. The errors in these experiments were due to the load cell, pressure transducers, DAQ, calibration, etc. All errors were analyzed by the method described in [20]. Both the bias uncertainty and the single sample precision were estimated in each variable. The major measurement inaccuracies of the data and performance parameters are presented in Table 1.

2.5. Data reduction

Some essential parameters such as the mass of the fuel and the dimensions of the nozzle before and after the test were measured. The pressure and temperature of the run tank, oxidizer mass flow rate, pressure of the combustion chamber, and the thrust were all evaluated and recorded during the test. The parameters of the engine's performance were calculated from the acquired data by using the following equations:

$$\bar{P}_c = \frac{\int_{t_i}^{t_f} P_c(t)\,dt}{(t_f - t_i)}, \tag{1}$$

$$\bar{T} = \frac{\int_{t_i}^{t_f} T(t)\,dt}{(t_f - t_i)}, \tag{2}$$

$$I_{sp} = \frac{\int_{t_i}^{t_f} T(t)\,dt}{(m_o + m_f)\,g}, \tag{3}$$

$$\overline{c^*} = \frac{\int_{t_i}^{t_f} P_c(t)\ A_t(t)\,dt}{(m_o + m_f)}, \tag{4}$$

$$\eta = \frac{\overline{c^*}}{c^*_{th}}, \tag{5}$$

$$\overline{O/F} = \frac{\int_{t_i}^{t_f} \dot{m}_o(t)\ dt}{\Delta m_f}, \tag{6}$$

$$\bar{\dot{r}} = \frac{\sqrt{\frac{m_{\text{final}} - m_{\text{initial}}}{\rho_f\ L\ \pi} + R^2_{\text{initial}}} - R_{\text{initial}}}{t_2 - t_1}, \tag{7}$$

$$\overline{G_o} = \frac{\int_{t_i}^{t_f} \dot{m}_o(t)\ dt}{(t_f - t_i)\ 0.25\,\pi\,((D_i + D_f)/2)^2}. \tag{8}$$

Table 1. Measurement inaccuracies.

Pressure (%)	**Thrust (%)**	$\dot{m}_{ox}$ **(%)**	I_{sp} **(%)**	C^* **(%)**	$\dot{r}$ **(%)**
0.14	0.22	0.74	0.81	0.81	0.33

2.6. A sample test

Figure 6 presents the motor during the firing test. To ease the discharging of the exhaust gas, a long tube in front of the plume was installed. Test conditions and results are shown in Table 2. Pressure of the chamber, thrust, and the injected oxidizer's flow of mass rate curves of this test are shown in Figure 7. As seen, inlet valve of the oxidizer was opened at $t = 6.7$ s, causing a slight increase in the motor's pressure of chamber. After a short time, approximately 0.2 s, firing command was sent to the igniter; when the igniter was activated, the fuel started to burn and pressure of the chamber rose rapidly, $t = 7.1$ s. From this moment until the stop command of the oxidizer, which was set at 7 s after opening the valve of the oxidizer (at $t = 13.7$ s), pressure of the chamber and the thrust remained constant. In a hybrid motor, the fuel regression rate is highly dependent on mass flux of the oxidizer through the port. However, as the fuel was regressed, and as the internal port diameter increased, mass flux of the oxidizer and the regression rate decreased. Increasing the fuel port diameter increased the burning surface. Nevertheless, as shown in Figure 7, the fuel mass flow rate did not change considerably.

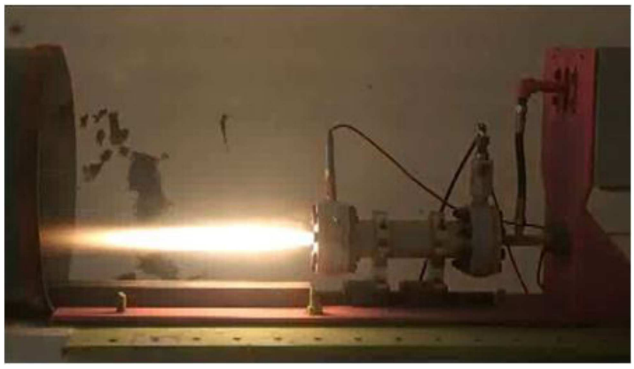

Figure 6. Hybrid motor during firing test.

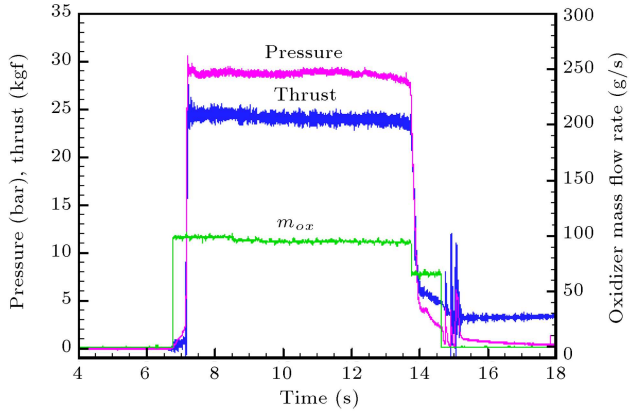

Figure 7. The results of a sample test.

As seen in Figure 7, at about 13.7 s, after the oxidizer had been cut off, the motor shut down immediately and the gases were discharged from the combustion chamber, leading to a sharp drop in the pressure and thrust. Note that after cutting off the oxidizer flow from running into the engine, the oxidizer was discharged from another line. Thus, after 13.7 s, a significant decrease (step) in the mass flow rate curve was observed due to the difference between the main-line and the discharge-line flow losses (Figure 7). Finally, the valve of the main oxidizer was cut off at $t = 14.7$ s and the mass flow rate tended towards zero. Immediately after this time, i.e. $t = 14.7$ s, a coolant gas (nitrogen) flowed into the motor to cool the internal components of the engine. However, since the coolant gas had entered the engine from a different line and had not passed through the flow meter, mass flow curve did not show any values. Nonetheless, the pressure and the thrust curves showed the existence of the flow in the engine during this period.

The results of this test show that the average fuel regression rate for the mean oxidizer's mass flux (6.88 g/cm^{2}s) is equal to 0.779 mm/s (Table 2). Actual, standard, and vacuum conditions of specific impulse are 204.6, 246.9, and 297.4 s, respectively, which are higher than the corresponding values for a solid rocket motor.

The fuel grains before and after the tests are shown in Figure 8. The grain that was cut indicated a non-uniform burning form along the length of the fuel, an issue that will be discussed later.

2.7. Data repeatability

To evaluate the repeatability of the results, the data gathered from three sample tests executed in the same conditions are shown in Figure 9. Figure 9 shows the pressure-time history; as seen, all three tests agree satisfyingly. The conditions, the results, and the compar-

Table 2. The sample test conditions.

Test no.	Fuel	Oxidizer	L_f (mm)	Initial D_p (mm)	Lpre (mm)	Lpost (mm)	ρ_f (kg/m^3)	A_{inj} (mm^2)	D_{th} (mm)	$\dot{m}_{ox}$ (g/s)	Initial m_f (g)	Final m_f (g)
26	HTPB	N2O	250.4	37.00	25	25	983	1.766	8.9	95.77	847.3	681.2

Final D_p (mm)	$\overline{G}_{ox}$ (g/cm^2 s)	$\overline{P}_c$ (bar)	$\bar{T}$ (kgf)	$\dot{m}_{\text{fuel}}$ (g/s)	$\dot{\bar{r}}$ (mm/s)	$\overline{OF}$	t_{burn} (s)	C^* (m/s)	C^*_{th} (m/s)	η	I_{sp} (s)	Standard I_{sp} (s)	Vacuum I_{sp} (s)
47.21	6.88	28.60	24.78	25.4	0.779	3.78	6.55	1513	1562	0.97	204.6	246.9	297.4

Table 3. Conditions and results of the reproducibility tests.

Test no.	L_{fuel} (mm)	$\dot{m}_{ox}$ (g/s)	t_{burn} (s)	$\overline{P}_c$ (bar)	$\overline{T}$ (kgf)	$\dot{m}_{\text{fuel}}$ (g/s)	$\overline{\dot{r}}$ (mm/s)	O/F	C^* (m/s)	I_{sp} (s)	Vacuum I_{sp} (s)
A1	249.0	66.51	6.61	19.95	15.37	22.68	0.732	2.93	1485	172.3	291.9
A2	249.0	67.35	6.48	19.86	15.11	22.93	0.721	2.94	1461	167.4	287.1
A3	250.0	68.75	6.33	20.25	15.94	23.90	0.745	2.88	1450	172.0	285.0
Average	249.3	67.54	6.47	20.02	15.47	23.17	0.733	2.92	1466	170.6	288.0
Standard deviation	0.577	1.133	0.140	0.204	0.425	0.646	0.012	0.034	17.934	2.787	3.524

(a) Before test (b) After test

Figure 8. The fuel grain before and after test.

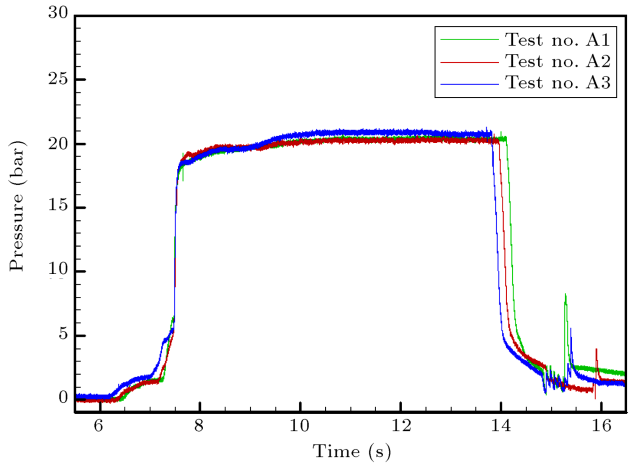

Figure 9. Pressure results for three different tests.

ison of the results of all test samples studied are listed in Table 3. It can be seen that the standard deviation of the data, shown in the last raw, is acceptable and the dispersion of the values is relatively low. For example, the maximum deviations from the average pressure, regression rate, and specific impulse are about 1.87%, 3.61%, and 3.13%, respectively, as shown in Table 3.

3. Regression rate correlation

The most important parameter in hybrid motors is the fuel regression rate and its relationship with other variables. Many theoretical and experimental studies have shown that the fuel regression rate in a hybrid motor is highly dependent on the mass flux passing through the fuel port [21-23]. Thus, in most studies, the regression rate only correlates with a parameter given by:

$$\dot{r} = a\, G_o^n. \tag{9}$$

For a fixed amount of fuel and oxidizer, it has been reported that the fuel regression weakly depends on the pressure of the combustion chamber, longitudinal distance from the edge of the fuel, and port diameter of the fuel [24-25].

To find the relationship between the fuel regression rate and mass flux of the oxidizer through the fuel port, several tests have been conducted. The conditions and results of the test are presented in Table 4. In all tests, the motor geometry and the fuel length (250 mm) were fixed. Various oxidizer mass fluxes in all tests were obtained by changing either the initial inner diameter of the fuel or the oxidizer mass flow rate. As a result, the mean oxidizer mass flux through the port varied between 3.5-12 g/cm^{2}s that covered the operation range of the present hybrid motor.

Table 4 presents the calculated ballistic parameters such as regression rate, the specific impulse, etc. Figure 10 shows variations of the regression rate with the oxidizer mass flux. Note that, unless specified, the term "regression rate" in this paper means both spatially and temporally averaged regression rates. It is observed that if these two parameters are plotted on logarithmic axes, a straight line can pass through almost all the acquired data, Figure 10. Therefore, the

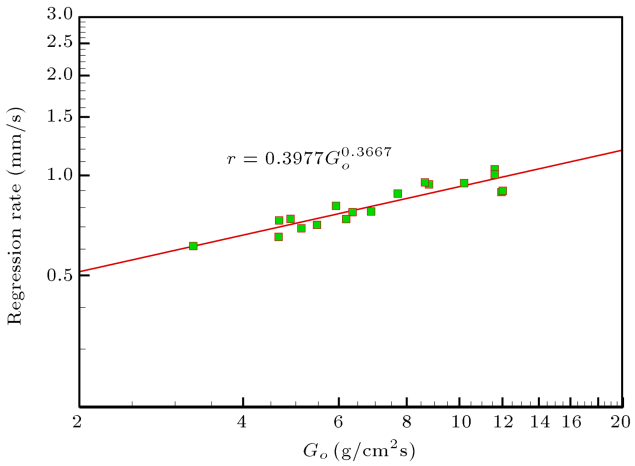

Figure 10. Regression rate versus oxidizer mass flux through the fuel port.

Table 4. Tests conditions and results for determining the regression rate correlation.

Test no.	$(D_{\text{port}})_{\text{initial}}$ (mm)	L_{fuel} (mm)	$(D_{\text{port}})_{\text{final}}$ (mm)	$\overline{\dot{m}}_{ox}$ (g/s)	t_{burn} (s)	$\overline{P}_c$ (bar)	$\overline{T}$ (kgf)	$\overline{\dot{m}}_{\text{fuel}}$ (g/s)	$\overline{\dot{r}}$ (mm/s)	O/F	$\overline{G}_{ox}$ (g/cm^{2}s)	C^* (m/s)	I_{sp} (s)
26	37.0	250.4	47.2	95.77	6.55	28.60	24.78	25.36	0.779	3.78	6.88	1514	204.6
43	26.3	250.0	37.7	96.15	6.41	28.26	25.30	21.91	0.891	4.39	11.95	1535	214.3
44	25.9	252.4	39.8	98.28	6.65	30.12	26.29	28.38	1.044	3.46	11.61	1522	207.6
47	39.8	249.0	42.4	101.98	1.50	30.96	29.12	28.40	0.882	3.59	7.70	1519	223.3
48	42.0	249.0	44.4	93.26	1.52	26.49	23.72	26.25	0.775	3.55	6.36	1424	198.5
49	44.4	249.0	46.7	96.70	1.44	29.31	25.56	28.96	0.810	3.34	5.93	1494	203.4
50	46.7	249.0	48.8	83.26	1.55	25.70	21.32	24.45	0.653	3.41	4.65	1535	197.9
51	48.8	249.0	50.7	94.97	1.33	29.07	24.55	28.87	0.740	3.29	4.89	1504	198.2
52	25.6	251.5	38.9	94.64	6.63	28.71	24.41	25.02	1.006	3.78	11.61	1538	204.0
54	25.9	248.5	38.4	71.23	6.63	20.86	17.04	21.93	0.940	3.25	8.79	1451	182.9
55	38.4	248.5	45.7	75.94	5.18	21.14	17.99	21.68	0.710	3.50	5.47	1403	184.3
58	26.0	251.0	37.7	95.64	6.49	27.69	24.48	20.99	0.899	4.56	12.02	1524	209.9
59	38.9	251.0	48.0	75.91	6.60	23.47	19.85	23.20	0.693	3.27	5.12	1528	200.3
63	37.5	251.0	47.4	87.43	6.67	25.64	22.91	22.98	0.739	3.80	6.19	1528	207.5
65	25.7	250.0	38.2	69.20	6.55	20.35	16.51	22.23	0.953	3.11	8.64	1477	180.6
67	25.4	250.0	37.8	79.92	6.54	24.52	20.56	21.87	0.948	3.65	10.20	1587	202.0
68	37.8	249.0	47.5	66.51	6.61	19.95	15.37	22.68	0.732	2.93	4.66	1485	172.3
69	47.5	249.0	55.4	67.32	6.48	19.87	15.07	22.95	0.613	2.93	3.24	1462	166.9

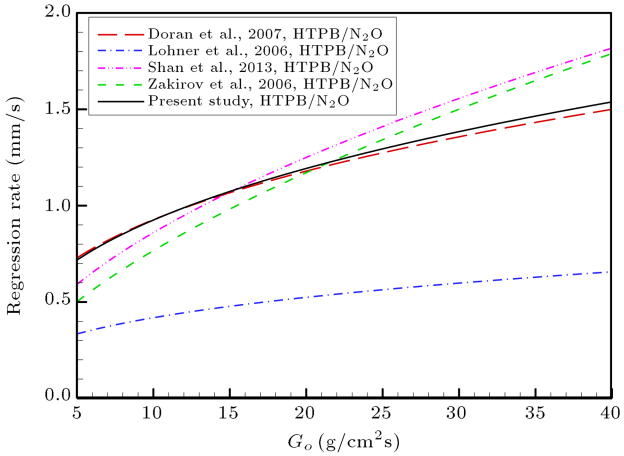

Figure 11. Comparison between the present result and other findings.

regression rate and the oxidizer mass flux are different from each other according to a power law equation given by:

$$\bar{\dot{r}} = 0.3977\bar{G}_o^{0.3667}. \tag{10}$$

Figure 11 compares the results of the new correlation, Eq. (10), with the results of pervious researchers. All studies have the same composition of fuel and oxidizer; however, other parameters are not similar. Therefore, the results are different. It is observed that the above correlation agrees very well with the relation presented by Doran et al. [2] that has approximately the same parameters as those in the present motor. Furthermore, Figure 11 clearly shows that for oxidizer mass flux above 25 g/cm^{2}s, the present method, Eq. (10), predicts a relatively accurate regression rate.

4. Fuel length effect

Several tests with various fuel lengths were conducted to investigate the effects of fuel length on the motor performance parameters, in particular the hybrid fuel regression rate. In these tests all conditions, such as oxidizer flow rate, port diameter, and motor geometry were held constant while only the fuel length was changed from 150 to 310 mm.

Figure 12 shows variation of the regression rate with the fuel length. It can be seen that the fuel regression rate increases almost linearly as the fuel length is increased. This is due to the increase in the total mass flux passing through the port that increases the heat transfer to the fuel surface.

The mass flow rate of oxidizer in all tests was held constant; therefore, variation of the fuel length changed the oxidizer to fuel mass ratio (O/F). The calculated characteristic velocity in the present measured data, C^*, is compared with that obtained from the equilibrium combustion code (CEA) results in Figure 13. The difference between the theoretical and experimental C^* determines the combustion efficiency. The resulted

combustion efficiencies are found to vary between 94 to 98%, which is within the range reported for hybrid motors.

Due to the significant effect of fuel length on the regression rate, it is necessary to develop a more general correlation for the hybrid fuel regression rate. Therefore, further tests were performed for different lengths and mass fluxes. Table 5 presents the results of these supplementary tests. Accordingly, the following equation is obtained, which shows a relation between the burning rate, the fuel length, and the oxidizer mass flux:

$$\bar{\dot{r}} = 0.07577\ \bar{G}_o^{0.364}\ L^{0.293}, \tag{11}$$

where $\bar{\dot{r}}$, G_o, and L are in mm/s, g/cm^{2}s, and mm, respectively. The above equation shows that regression rate is strongly dependent on the fuel length, though it is marginally less dependent on the mass flux. This relation is plotted in Figure 14 and shows that the maximum regression rate occurs at both maximum oxidizer mass flux and fuel length.

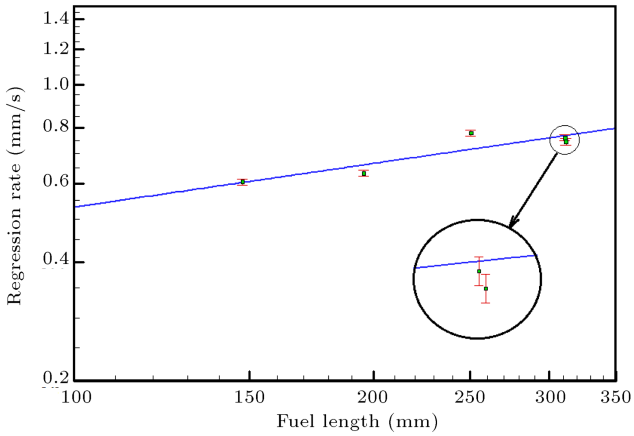

Figure 12. Fuel burning rate relation with the fuel length.

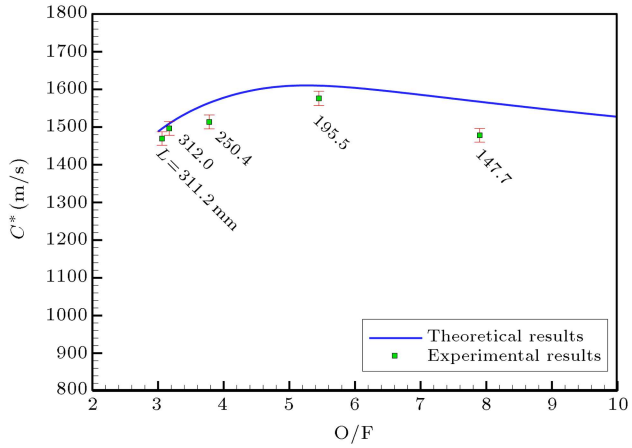

Figure 13. Comparison of theoretical and experimental characteristic velocities.

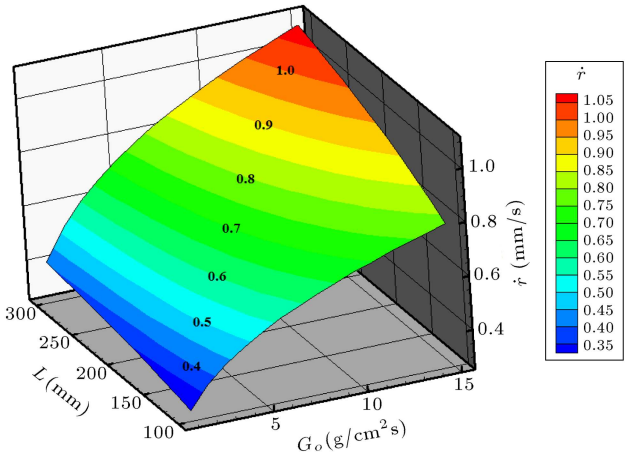

Figure 14. Regression rate versus fuel length and oxidizer mass flux.

5. The effect of combustion chamber pressure

In solid composite motors, the chamber pressure has a significant effect on the internal ballistics and the

Table 5. The results of supplementary tests for different lengths and oxidizer mass fluxes.

Test no.	L_{fuel} (mm)	$\bar{\dot{m}}_{ox}$ (g/s)	t_{burn} (s)	$\bar{P}_c$ (bar)	$\bar{T}$ (kgf)	$\bar{\dot{m}}_{\text{fuel}}$ (g/s)	$\bar{\dot{r}}$ (mm/s)	O/F	$\bar{G}_{ox}$ (g/cm^2.s)	C^* (m/s)	I_{sp} (s)	Standard I_{sp} (s)	Vacuum I_{sp} (s)
20	147.7	88.62	6.64	22.85	17.82	11.22	0.605	7.90	6.83	1478	178.5	241.1	290.5
21	195.5	84.46	6.57	24.45	15.79	15.49	0.633	5.45	6.54	1576	158.0	257.1	309.7
23	312.0	94.62	6.54	29.06	21.56	29.82	0.745	3.17	6.94	1496	173.3	244.1	294.0
24	311.2	94.42	6.58	28.73	22.89	30.90	0.760	3.06	6.67	1469	182.7	239.7	288.8
56	250.0	106.48	4.69	31.80	28.24	22.84	0.654	4.66	6.62	1572	218.4	256.4	308.8
62	310.0	95.40	6.63	28.28	25.65	29.20	1.007	3.27	11.85	1488	205.9	242.8	292.5
64	251.0	83.39	6.59	24.90	21.39	21.50	0.557	3.88	3.83	1563	203.9	255.0	307.2
66	250.0	83.10	6.54	24.88	21.59	21.54	0.691	3.86	5.80	1566	206.3	255.4	307.6
70	250.0	72.36	6.33	21.46	16.66	23.90	0.802	3.03	5.53	1476	173.1	240.8	290.0
71	202.0	73.83	5.83	22.04	17.50	18.70	0.662	3.95	4.11	1576	189.1	257.0	309.6
72	201.8	67.39	6.31	19.98	15.81	17.34	0.643	3.89	4.10	1566	186.6	255.4	307.7

Table 6. Test conditions and results for different throat diameters (different chamber pressures).

Test no.	D_{th} (mm)	$(D_{port})_{initial}$ (mm)	L_{fuel} (mm)	$\overline{\dot{m}}_{ox}$ (g/s)	t_{burn} (s)	$\overline{P}_c$ (bar)	$\overline{T}$ (kgf)	$\overline{\dot{m}}_{fuel}$ (g/s)	$\overline{\dot{r}}$ (mm/s)	O/F	C^* (m/s)	I_{sp} (s)	Standard I_{sp} (s)	Vacuum I_{sp} (s)
54	8.90	25.9	248.5	71.23	6.63	20.86	17.04	21.93	0.940	3.25	1451	182.9	236.7	285.1
65	9.00	25.7	250.0	69.20	6.55	20.35	16.51	22.23	0.953	3.11	1476	180.6	240.9	290.1
73	10.50	26.1	251.0	64.38	6.54	14.19	13.20	21.39	0.910	3.01	1521	153.9	248.1	298.9
74	7.50	26.0	251.0	72.55	6.69	31.81	17.73	20.38	0.874	3.56	1553	190.8	253.4	305.2

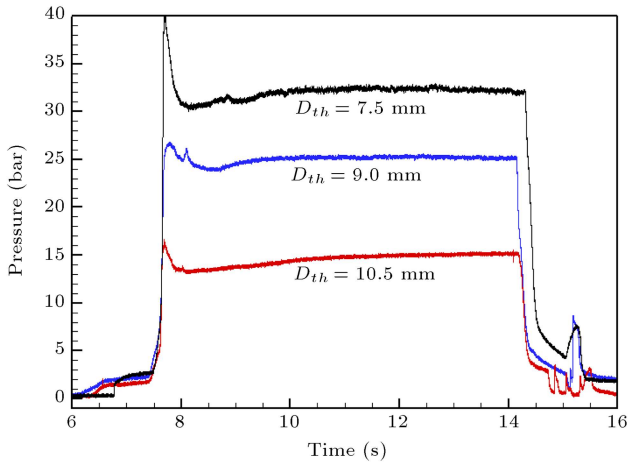

Figure 15. Effect of throat diameter on the combustion pressure.

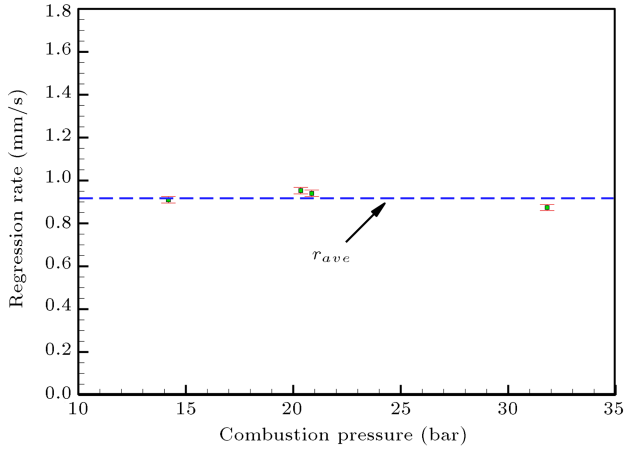

Figure 16. Variation of the fuel regression rate with chamber pressure.

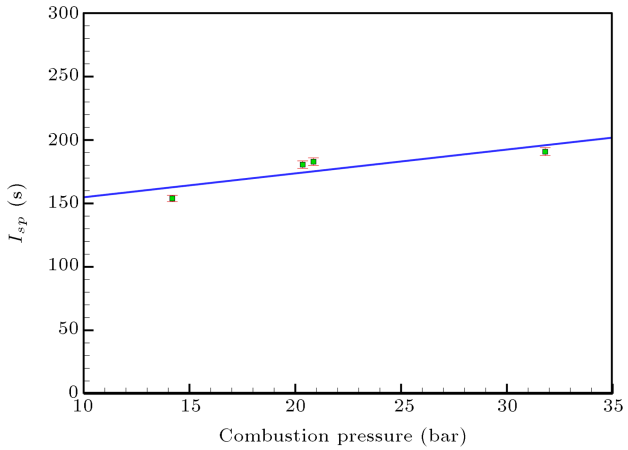

Figure 17. Effect of combustion pressure on the specific impulse.

burning rate highly depends on the chamber pressure. However, the effect of pressure is not significant in hybrid motors and it is often ignored. To further investigate the pressure effects, by keeping all test conditions constant, only the nozzle throat varies in different tests so that the combustion can be established at different pressures. The conditions of these tests are presented in Table 6.

The pressure curves for three different throat diameters, 7.5, 9.0, and 10.5 mm, are shown in Figure 15. Obviously, high combustion chamber pressure is obtained for the smaller nozzle throat diameter, D_{th} = 7.5 mm. The corresponding regression rates derived from these tests are shown in Figure 16. According to this figure, the combustion chamber pressure does not have any significant effect on the regression rate and, as seen in Figure 16, the maximum deviation from a mean value is about 5%. However, the specific impulse increases considerably as the chamber pressure increases, Figure 17. This is due to the increase in the thrust coefficient (C_F) with pressure that creates a higher thrust [1].

6. Local regression rate

The calculated values for the regression rate in the previous sections were based on the average values over the entire length of the fuel. However; due to the varying conditions along the fuel port, the regression rate might not be uniform. To study this variation, a grain was cut after the test and the amount of regressed fuel was measured in different sections along the port. Thus, to spatially indicate the varying regression rate, the local fuel regression rate was calculated. Figure 18 shows the internal surface of the fuel port before and after each sample test. It is observed that the amount of regressed fuel at the beginning of grain is low and it gradually increases to a maximum value around $x/L = 0.4$. After this point, the amount of regressed fuel decreases until the end of the fuel grain, $x/L = 1.0$.

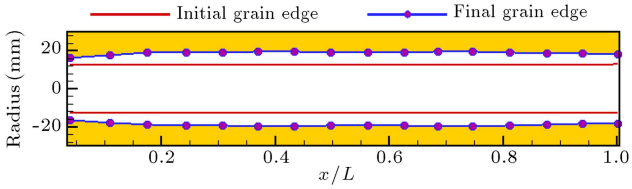

Figure 18. The fuel port shape before and after the test.

The regression rates were calculated for various sections that had the same quantitative patterns of regressed fuel; the results are plotted in Figure 19. The lowest value of regression rate is in the beginning of the fuel, i.e. injector side, about 0.6 mm/s. It differs by about 37.5% from its average value, 0.96 mm/s. Furthermore, the maximum value is about 1.06 mm/s that differs by about 10.4% from its average value. In fact, the local fuel burning rate in the major part of the fuel length (about 83% of the total) has only ± 10% deviation from the mean burning rate value. Only in the initial and final parts of the fuel port, the deviation from the mean value is significant. Hence, the dependency of the fuel regression rate on the longitudinal distance has been neglected and only local average value of the regression rate is considered in most of the tests in this field. Thus, the following correlation can be considered for the local regression rate of the present test:

$$\dot{r}(x) = 0.537 + 2.665\left(\frac{x}{L}\right) - 3.968\left(\frac{x}{L}\right)^2 + 1.596\left(\frac{x}{L}\right)^3. \quad (12)$$

In addition, the following general correlation for the local fuel regression rate based on the measurements in several fuel cuts is obtained:

$$\dot{r}(x) = 0.07577\ \bar{G}_o^{0.364}\ L^{0.293}\left(0.559 + 2.776\left(\frac{x}{L}\right) - 4.133\left(\frac{x}{L}\right)^2 + 1.662\left(\frac{x}{L}\right)^3\right). \quad (13)$$

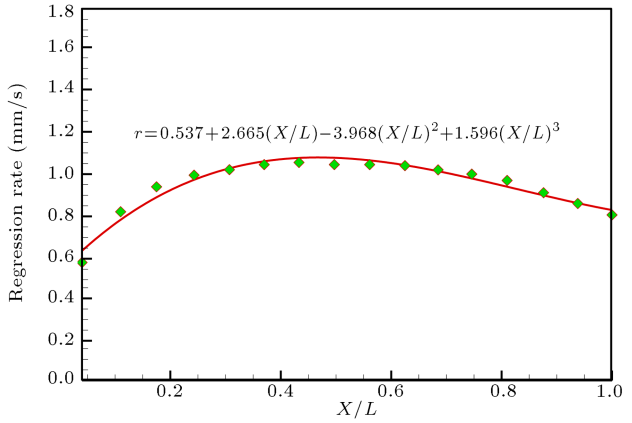

Figure 19. Fuel regression rate in different sections.

7. Temporal (instantaneous) regression rate

There are a few methods than could be used to measure the instantaneous fuel regression rate, e.g. an instantaneous scan of motor during its operation or using ultrasonic sensors. Note that in the second scheme, the instantaneous thickness of the fuel during the test is measured and from this value, the temporal regression rate is calculated.

However, both of the aforementioned methods require expensive equipment and the most active research groups in the field of hybrid propulsion systems are incapable of providing the costs of these tools. Therefore, the fuel regression rate has been calculated based on an average form, which gives an acceptable accuracy. In all the mentioned test results, the temporal average of regression rates is calculated and presented. However, in this section, the instantaneous regression rate is obtained by a special method and is compared with the temporal average regression rate.

A sample fuel grain is tested in short time intervals and the fuel regression (new geometry of fuel) is measured after each test. In this way, the fuel regression at different time intervals is measured and, from this measurement, the instantaneous regression rate is obtained. This method is similar to a long-time test where the time is frozen at a certain moment, which enables the fuel regression measurement. According to this approach, a fuel sample with the characteristics listed in Table 7 was tested. The time for each test was about 1.5 s where once this time elapsed, the oxidizer was automatically cut off and the motor was extinguished. Then, the remaining fuel was removed and the remaining fuel mass and dimensions were measured. Once all the necessary measurements were finished, the fuel was put back in the motor and the test was resumed for another 1.5 s under conditions similar to the previous test. This procedure was repeated 6 times and, for each time, the fuel mass and dimensions were measured. Figure 20 shows the diameter of the fuel at different times. As seen in the measured data, in a logarithmic scale, the variation is exactly linear and the following curve fit can be obtained:

$$D(t) - D_0 = 2.144\ t^{0.8474}. \quad (14)$$

Based on the definition, the instantaneous fuel regression rate (burning rate) can be calculated from the following equation:

$$\dot{r}(t) = \frac{d\left(D(t) - D_0\right)}{2\,dt} = \frac{d\left(2.144\ t^{0.8474}\right)}{2\,dt} = 0.9084\,t^{-0.1526}. \quad (15)$$

The above regression rate relation is plotted in Figure 21. It is seen that with increasing time, the regression rate decreases, which is caused by the reduction

Table 7. The initial tested fuel specification to achieve instantaneous regression rate.

Fuel	Oxidizer	L_f (mm)	Initial D_p (mm)	Lpre (mm)	Lpost (mm)	ρ_f (kg/m^3)	A_{inj} (mm^2)	D_{th} (mm)	D_{ex} (mm)	Initial m_f (g)
HTPB	N_2O	249	36.9	25	25	1003	1.766	8.9	22.4	847.3

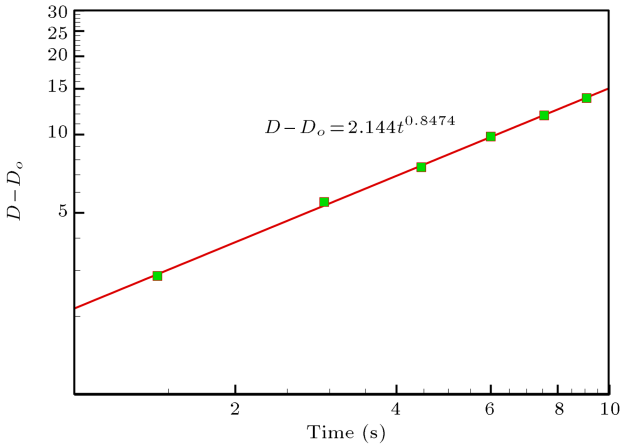

Figure 20. Fuel port diameter versus time.

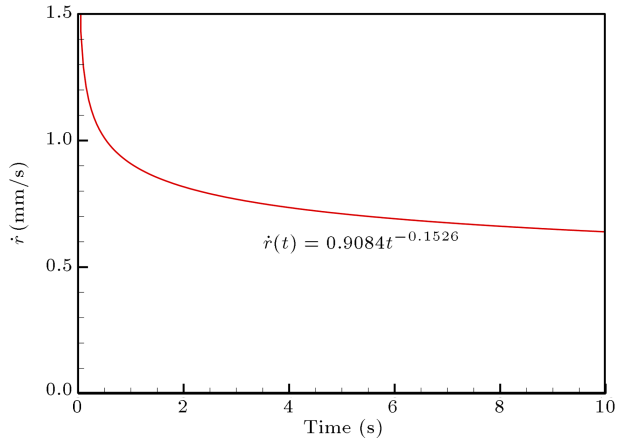

Figure 21. Instantaneous fuel regression rate.

in the oxidizer mass flux. This is because the port diameter increases with increasing both the time and burning of fuel.

8. Conclusion

The effects of various parameters on the fuel regression rate of an HTPB/N_2O hybrid motor were experimentally investigated. It was observed that the most important parameter affecting the regression rate was the oxidizer mass flux passing through the fuel port that varied with a power law equation. Moreover, the fuel length had a significant effect on the regression rate; however, the effect of combustion chamber pressure was negligible. Further, a correlation between the fuel regression rate and the oxidizer mass flux and the fuel length was obtained. In addition, the amount of regressed fuel along the grain was measured and the local regression rate was calculated. It was observed that the highest value of burning rate occurred at a distance of about one-third the fuel length from the beginning of the fuel edge. Finally, a special technique was used to calculate the instantaneous regression rate and it was shown that the variation, in a logarithmic scale, was linear.

Acknowledgement

This project was financially supported by the Space Transportation Research Institute-Iranian Space Research Center, which is greatly appreciated.

Nomenclature

a	Regression rate coefficient
A_{th}	Nozzle throat area, mm^2
C_F	Thrust coefficient
C^*	Characteristic velocity, m/s
$\overline{C^*}$	Average characteristic velocity, m/s
C^*_{th}	Theoretical characteristic velocity, m/s
D	Fuel port diameter, mm
D_f	Final port diameter, mm
D_i	Initial port diameter, mm
D_0	Initial diameter, mm
D_{th}	Throat diameter, mm
G	Mass flux, g/cm^{2}s
G_o	Oxidizer mass flux, g/cm^{2}s
$\overline{G_o}$	Average oxidizer mass flux, g/cm^{2}s
I_{sp}	Specific impulse, s
L	Characteristic length, mm
m_f	Fuel mass, g
m_o	Oxidizer mass, g
m_{final}	Final mass, g
m_{initial}	Initial mass, g
$\dot{m}_f$	Fuel mass flow rate, g/s
$\dot{m}_o$	Oxidizer mass flow rate, g/s
n	Regression rate coefficient
O/F	Oxidizer to fuel ratio
$\overline{O/F}$	Average oxidizer to fuel ratio

P_c	Combustion chamber pressure, Pa
$\overline{P_c}$	Average combustion chamber pressure, Pa
R	Fuel port radius, mm
$\dot{r}$	Local regression rate of fuel, mm/s
$\overline{\dot{r}}$	Average regression rate of fuel, mm/s
t	time, s
t_f	Final time, s
t_i	Initial time, s
T	Thrust, N
$\overline{T}$	Average thrust, N
x	Distance, mm
ρ_f	Density of solid fuel, kg/m^3
η	Combustion efficiency
γ	Specific heat ratio
π	Pi number, 3.1415

References

1. Rezaei, H. and Soltani, M.R. "An analytical and experimental study of a hybrid rocket motor", *Proc IMechE Part G: J Aerospace Engineering*, **228**(13), pp. 2475-2486 (2014).
2. Doran, E., Dyer, J., Dunn, Z., et al. "Nitrous oxide hybrid rocket motor fuel regression rate characterization", *AIAA Paper*, pp. 2007-5352 (2007).
3. Connel, T.L., Santi, S.A., Risha, G.A. et al. "Experiment and semi-empirical modeling of lab-scale hybrid rocket performance", *AIAA Paper*, pp. 2009-5086 (2009).
4. http://www.scaled.com/projects/tierone/
5. Cavalleri, R.J. and Loehr, R.D. "Hybrid rocket propulsion performance prediction", *AIAA Paper*, pp. 2005-3548 (2005).
6. Zilliac, G. and Karabeyoglu, M.A. "Hybrid rocket fuel regression rate data and modeling", *AIAA Paper*, pp. 2006-4504 (2006).
7. Yen-Sen, C., Lian, Y.Y., Yang, L. and Wu, B. "Combustion modeling and analysis of hybrid rocket motor internal ballistics", *AIAA Paper*, pp. 2012-3749 (2012).
8. Kim, J., Kim, S., Kim, J. and Moon, H. "Experimental investigations of the tapered fuel regression rate of a hybrid rocket motor", *AIAA Paper*, pp. 2010-7119 (2010).
9. Risha, G.A., Evans, B.J., Boyer, E., Wehrman, R.B. and Kuo, K.K. "Nano-sized aluminum and boron-based solid fuel characterization in a hybrid rocket engine", *AIAA Paper*, pp. 2003-4593 (2003).
10. Aoki, A. and Fukuchi, A. "Development of low cost fuels for hybrid rocket engine", *AIAA Paper*, pp. 2010-6638 (2010).
11. Estey, P., Altman, D. and Mc Farlane, J. "An evaluation of scaling effects for hybrid rocket motors", *AIAA-91-2517* (1991).
12. Karabeyoglu, A., Zilliac, G., Cantwell, B.J., DeZilwa, S. and Castellucci, P. "Scale-up tests of high regression rate paraffin-based hybrid rocket fuels", *Journal of Propulsion and Power*, **20**(6), pp. 1037-1045 (2004).
13. George, P., Krishnan, S., Varkey, P.M., Ravindran, M. and Ramachandran, L. "Fuel regression rate in hydroxyl-terminated-poly butadiene/gaseous-oxygen hybrid rocket motors", *Journal of Propulsion and Power*, **17**(1) (2001).
14. Gomes, S.R., Rocco Junior, L., Rocco, J.A.F.F. and Iha, K. "Gaseous oxygen injection effects in hybrid labscale rocket motor operations", *AIAA Paper*, pp. 2010-6545 (2010).
15. Potapkin, A.V. and Lee, T.S. "Experimental study of thrust performance of a hybrid rocket motor with various methods of oxidizer injection", *Combustion, Explosion, and Shock Waves*, **40**(4), pp. 386-392 (2004).
16. Peretz, A., Einav, O., Hashmonay, B., Birnholz, A. and Sobe, Z. "Development of a laboratory-scale system for hybrid rocket motor testing", *Journal of Propulsion and Power*, **27**(1), pp. 190-196 (2011).
17. Lohner, K., Dyer, J., Doran, E., Dunn, Z. and Zilliac, G. "Fuel regression rate characterization using a laboratory scale nitrous oxide hybrid propulsion system", *AIAA Paper*, pp. 2006-4671 (2006).
18. Shan, F., Hou, L. and Piao, Y. "Combustion performance and scale effect from N_2O/HTPB hybrid rocket motor simulations", *Acta Astronautica Journal*, **2013**(85), pp. 1-11 (2013).
19. Swami, R.D. and Gany, A. "Analysis and testing of similarity and scale effects in hybrid rocket motors", *Acta Astronautica*, **2003**(52), pp. 619-628 (2003).
20. Beckwith, T.G., Maraugoni, R.D. and Lienhard, V.J.H., *Mechanical Measurements*, 5th Ed. Cambridge, MA: Addison-Wesley Publishing Company (1993).
21. Sutton, G.P. and Biblarz, O., *Rocket Propulsion Elements*, 7th Ed, John Wiley & Sons (2001).
22. Carmicino, C. and Sorge, A.R. "Influence of a conical axial injector on hybrid rocket performance", *Journal of Propulsion and Power*, **22**(5), pp. 984-995 (2006).
23. Farbar, E., Louwers, J. and Kaya, T. "Investigation of metalized and non metalized hydroxyl terminated poly butadiene/hydrogen peroxide hybrid rockets", *Journal of Propulsion and Power*, **23**(2), pp. 476-486 (2007).
24. Frederick, R.A. and Whitehead, J.J. "Predicting hybrid propellant regression rate using response surfaces", *Journal of Propulsion and Power*, **25**(3), pp. 815-818 (2009).
25. Patnala, S., Chattaraj, T. and Joshi, P.C. "Combustion studies on paraffin wax in gaseous oxygen and nitrous oxide", *ARPN Journal of Engineering and Applied Sciences*, **7**(7), pp. 806-811 (2012).

Biographies

Hadi Rezaei received his PhD degree in Mechanical Engineering in the field of Energy Conversion. Now, he is a Senior Researcher at Space Transportation Research Institute, Iranian Space Research Center. His favorites include hybrid motor, energy conversion, intake flows, and propulsion.

Mohammad Reza Soltani is a Professor in the Aerospace Engineering Department of Sharif University of Technology, Tehran, and has a PhD in Applied Aerodynamics from University of Illinois, Urbana-Champaign, 1991, USA. His research interests include applied aerodynamics, unsteady aerodynamics, design and building of wind tunnels and wind turbines, and measurement methods.

Ali Reza Mohammadi achieved his PhD degree in Mechanical Engineering in the field of Energy Conversion. Now, he is a Senior Researcher at Space Transportation Research Institute, Iranian Space Research Center. His favorites include combustion, energy conversion, and propulsion.